

Detection of Gamma-rays around 1 TeV from RX J0852.0–4622 by CANGAROO-II

H. Katagiri¹, R. Enomoto², L.T. Ksenofontov², M. Mori², Y. Adachi², A. Asahara¹,
G.V. Bicknell³, R.W. Clay⁴, Y. Doi⁵, P.G. Edwards⁶, S. Gunji⁵, S. Hara², T. Hara⁷,
T. Hattori⁸, Sei. Hayashi⁹, C. Itoh¹⁰, S. Kabuki², F. Kajino⁹, A. Kawachi², T. Kifune¹¹,
R. Kiuchi², H. Kubo¹, T. Kurihara⁸, R. Kurosaka², J. Kushida⁸, Y. Matsubara¹²,
Y. Miyashita⁸, Y. Mizumoto¹³, H. Muraishi¹⁴, Y. Muraki¹², T. Naito⁷, T. Nakamori¹,
T. Nakase⁸, D. Nishida¹, K. Nishijima⁸, M. Ohishi², K. Okumura², J.R. Patterson⁴,
R.J. Protheroe⁴, N. Sakamoto⁵, Y. Sakamoto⁸, D.L. Swaby⁴, T. Tanimori¹, H. Tanimura¹,
G.J. Thornton⁴, K. Tsuchiya², S. Watanabe¹, T. Yamaoka⁹, S. Yanagita¹⁵, T. Yoshida¹⁵,
T. Yoshikoshi²

ABSTRACT

We have detected gamma-ray emission at the 6σ level at energies greater than 500 GeV from the supernova remnant RX J0852.0–4622 (G266.2–1.2) using the

¹Department of Physics, Graduate School of Science, Kyoto University, Sakyo-ku, Kyoto 606-8502, Japan; katagiri@cr.scphys.kyoto-u.ac.jp, enomoto@icrr.u-tokyo.ac.jp

²Institute for Cosmic Ray Research, University of Tokyo, Kashiwa, Chiba 277-8582, Japan

³RSAA, Australian National Univ., ACT 2611, Australia

⁴Dept. of Physics, Univ. of Adelaide, SA 5005, Australia

⁵Department of Physics, Yamagata University, Yamagata, Yamagata 990-8560, Japan

⁶Institute of Space and Astronautical Science, Japan Aerospace Exploration Agency, Sagami-hara, Kanagawa 229-8510, Japan

⁷Faculty of Management Information, Yamanashi Gakuin University, Kofu, Yamanashi 400-8575, Japan

⁸Department of Physics, Tokai University, Hiratsuka, Kanagawa 259-1292, Japan

⁹Department of Physics, Konan University, Kobe, Hyogo 658-8501, Japan

¹⁰Ibaraki Prefectural University of Health Sciences, Ami, Ibaraki 300-0394, Japan

¹¹Faculty of Engineering, Shinshu University, Nagano, Nagano 480-8553, Japan

¹²Solar-Terrestrial Environment Laboratory, Nagoya University, Nagoya, Aichi 464-8602, Japan

¹³National Astronomical Observatory of Japan, Mitaka, Tokyo 181-8588, Japan

¹⁴School of Allied Health Sciences, Kitasato University, Sagami-hara, Kanagawa 228-8555, Japan

¹⁵Faculty of Science, Ibaraki University, Mito, Ibaraki 310-8512, Japan

CANGAROO-II Imaging Atmospheric Cherenkov Telescope (IACT). The flux was 0.12 times of that of Crab at 1 TeV. The signal centroid is consistent with the peak of the X-ray emission in the north-west rim of the remnant.

Subject headings: gamma rays: observation — (stars:) supernovae: individual (RX J0852.0–4622)

1. Introduction

Young supernova remnants (SNRs) have for many years been believed to accelerate cosmic rays up to energies around the “knee” of the cosmic ray spectrum at ~ 100 TeV, however direct observational evidence has only recently been found to support this. The interactions of such high energy cosmic rays with surrounding material produce a signature in TeV energy gamma-rays, and so TeV observations of SNR are therefore of fundamental importance in understanding the origin of Galactic cosmic rays. To date, the only SNRs which have been reported to emit TeV gamma-rays are the shell-type SNRs SN1006 (Tanimori et al. 1998), RX J1713.7–3946 (Muraishi et al. 2000; Enomoto et al. 2002b), and Cassiopeia A (Aharonian et al. 2001). However, although RX J1713.7–3946 has been detected by two groups (Hofmann 2004), there have as yet been no confirming reports for Cassiopeia A, and for SN1006, a recent upper limit is significantly below the originally reported flux (Hofmann 2004). Therefore, in addition to further observations of these sources, it is necessary to search for further examples of such SNRs.

RX J0852.0–4622 (G266.2–1.2) is a SNR located (in projection) at the southeast corner of the Vela SNR. It was discovered by Aschenbach (1998) using data from the *ROSAT* All-Sky Survey. It is one of the few known SNRs which display strong non-thermal X-ray emission (Tsunemi et al. 2000; Slane et al. 2001). In addition, the 1157 keV line of ^{44}Ti was detected by COMPTEL (Iyudin et al. 1998). From a consideration of the lifetime of ^{44}Ti (~ 90 yr), the X-ray flux, and the angular size of the X-ray emission, $\sim 2^\circ$, the age and distance from the Earth were estimated to be 500–1100 yr and 80–500 pc, respectively (Aschenbach, Iyudin, & Schonfelder 1999). An independent estimate of the distance, of 1–2 kpc, was provided by Slane et al. (2001) from a simple scaling of the column density, which suggested that the SNR was at least several times more distant than the Vela SNR. *ASCA* hard X-ray images revealed a shell-like morphology with a featureless spectrum well described by a power-law (Tsunemi et al. 2000; Slane et al. 2001). Radio emission also has a non-thermal spectrum (Combi, Romero, & Benaglia 1999; Duncan & Green 2000). Both the X-ray and radio emission are brightest in the north-west rim of the SNR. These data suggest that particles may be being accelerated to ~ 100 TeV. At these energies electrons can give rise to TeV gamma-rays

through inverse Compton scattering, and protons can interact with surrounding material to produce TeV gamma-rays via π^0 decay.

Furthermore, RX J0852.0–4622 is, like RX J1713.7–3946, an extended SNR at X-ray energies. The relatively large angular size enables us to study the detailed morphology even with the existing angular resolution.

We have observed RX J0852.0–4622 with the 10 m diameter CANGAROO-II Imaging Atmospheric Cherenkov Telescope (IACT). The telescope (Kawachi et al. 2001) detects gamma-rays above several hundred GeV by reconstructing optical Cherenkov images generated by relativistic secondary particles in the cascades produced when high-energy gamma-rays (and background cosmic rays) interact with the Earth’s upper atmosphere. Parametrizing the optical images enables the direction and energy of gamma-ray events to be inferred. The telescope is located near Woomera, South Australia ($136^{\circ}47' \text{ E}$, $31^{\circ}06' \text{ S}$), from which RX J0852.0–4622 culminates at $\sim 15^{\circ}$ from the zenith, enabling observations with a lower energy threshold. The angular resolution of CANGAROO-II was estimated to be $0.30\text{--}0.39^{\circ}$ ($2.6\text{--}3.4 \text{ pc}$ at a distance of 0.5 kpc) with an energy threshold of 500 GeV depending on the observing conditions and the spectrum.

2. Observations

The observations were carried out between 2001 December 12 and 2002 February 15 (19 nights), and between 2003 January 5 and February 28 (25 nights). The telescope tracked the peak of the X-ray emission, in the north-west rim of the SNR ($\alpha = 132.25^{\circ}$, $\delta = -45.65^{\circ}$, J2000 coordinates). The field of view (FOV) of the camera is $2.76^{\circ} \times 2.76^{\circ}$. The brightest star in the FOV, SAO 220422, has a visual magnitude of 4.1, and this region is brighter than our typical on-source FOV. As a result, we used a higher trigger threshold, requiring 5 triggered pixels rather than the usual 3 (Itoh et al. 2003). The recently installed lights several kilometers from the telescope were expected to have little effect on these observations as the telescope was pointed close to the zenith (Itoh et al. 2003), and this was confirmed from the azimuthal angle dependence of the shower rate (see §3). Each night was divided into two or three periods, i.e., ON–OFF, OFF–ON–OFF, or OFF–ON observations. ON-source observations were timed to contain the meridian passage of the target, as was done by Enomoto et al. (2002b). In total, 5900 min. of ON- and 5300 min. of OFF-source data were obtained.

3. Analysis

First, ‘cleaning’ cuts on camera images were applied, requiring (0.115°-square) pixel pulse-heights of greater than 3.3 photoelectrons, and Cherenkov photon arrival times within ± 50 ns of the median arrival time. Clusters of at least five adjacent triggered pixels (rather than the usual four-pixel cut) were required in each event to minimize the effects of the bright star field. After these pre-selection cuts, which reduced events due to background light were reduced by 99%, the shower rate was stable on a run-to-run basis for observations in the same year. The systematic difference of the run-by-run acceptance within the same year is expected to be less than 12%. The ON/OFF shower rate differences in 2002 and 2003 were $-8 \pm 15\%$ and $-1 \pm 13\%$, respectively. By examining the event rates within each run we were able to reject periods affected by cloud, dew forming on the mirrors, instrumental abnormalities, etc. Only data taken at elevation angles greater than 60° were accepted. After these cuts, 4300 min. of ON- and 3900 min. of OFF-source data survived.

Trigger rates for each pixel per $700 \mu\text{s}$ were monitored by a scaler circuit in real-time and recorded each second. These data were used to exclude ‘hot’ pixels (generally due to the passage of a star through the FOV of a pixel) in off-line analysis. Hillas parameters were then calculated to discriminate gamma-rays from cosmic rays based on the image shape and orientation (Hillas 1985). Further, in each year’s data, we masked a small number of pixels which showed deformed ADC spectra, possibly due to a hardware fault. Discrimination of the cosmic ray background from gamma-rays was carried out using the likelihood method of Enomoto et al. (2002a).

4. Results

The resulting distributions of the image orientation angle, α , for the combined data in 2002 and 2003 are shown in Fig. 1. The normalizations between the ON- and OFF-distributions were carried out using data with $\alpha > 27^\circ$. The numbers of excess events ($\alpha < 18^\circ$) were 530 ± 120 (in an observation time of 2100 min.), 540 ± 140 (2200 min.), and 1080 ± 180 (4300 min.) in 2002, 2003, and the combined data, respectively. The excess rates for 2002 and 2003 were similar to each other. Nightly signal rates were also checked during both years. The largest deviations occurred with a rate 2.5 ± 0.9 times larger than the average for 2002 and 3.0 ± 1.0 times for 2003, respectively. These are not unexpected statistically, and therefore there is no evidence of time-variability in the TeV emission.

To check on the spatial distribution of the signal we derived the ‘significance map’, shown by the blue contours in Fig. 2. The contours were calculated from the distribution of

the detection significance determined at each location from the difference in the α plots (ON-minus OFF-source histogram) divided by the statistical errors. The centroid is consistent with position of the X-ray maximum, within our possible systematic uncertainty of 0.1° . The region enclosed by the 65% (of the peak TeV significance) contour is elliptical with a semi-minor axis of 0.19° (NE-SW) and a semi-major axis of 0.35° (NW-SE), while our angular resolution was estimated to be $0.30\text{--}0.39^\circ$. The acceptance of the CANGAROO-II telescope decreases smoothly with offset from the tracking center, falling to 50% at a 0.9° offset, i.e. at the edge of the trigger region. It is difficult to obtain the reliable upper limits on the two neighboring X-ray enhancements in the rim since they are near the edge of the trigger region.

After correcting for this acceptance, the differential fluxes listed in Table 1 were derived. As both statistical and systematic errors are included, the energy bins overlap somewhat, particularly at low energies. The systematic uncertainty for the energy determination ($\sim 20\%$) dominates the errors in the energies. The Spectral Energy Distributions (SEDs), derived from radio, X-ray, MeV gamma-ray, and our TeV gamma-ray observations, are plotted in Fig. 3. The hatched area indicates the allowed region, where the χ^2 for the power-law fitting $< \chi_{\min}^2 + 1$ including energy uncertainty, and χ_{\min}^2 is the χ^2 for the best fit. The values are listed in Table 1. The derived spectrum has a power-law index of $-4.3_{-4.4}^{+1.7}$, the errors of which come predominantly from the uncertainty in energy.

The derived spectrum from RX J0852.0–4622 seems rather steep. The photon index of -2.6 , however, is within 1σ level due to the large uncertainty on the energy determination. This indicates that we cannot firmly conclude that the energy spectrum as soft as spectral index of -4.3 . Recently CANGAROO-II collaboration has reported a similar steep spectrum from the Galactic Center (Tsuchiya et al. 2004). This spectrum is different from that reported by H.E.S.S. collaboration (Aharonian et al. 2004a). Applying the same procedure to the Galactic Center result, the allowed spectral index range became $-4.6_{-5.0}^{+1.2}$. No further answer on this is found in this stage. Time variability might be one of solution (Aharonian & Neronov 2004). On the other hand, the difference in the energy spectrum from the SNR RX J1713.7–3946 between the CANGAROO-II and the H.E.S.S. is 2.2σ level (Aharonian et al. 2004b). These complex situations encourage the further observations and analysis of the stereoscopic data using IACTs.

Our Monte Carlo simulations predict, even for a point-source, that the α distribution of gamma-ray events for this soft spectrum should have a broader peak than that for a Crab-like spectrum. Therefore we cannot conclude from the experimental data whether this source is extended or point-like.

Various checks on the signal yield and position were carried out, by varying thresh-

olds, clustering cuts, Hillas parameter values, etc: these yielded consistent fluxes within the systematic errors given in Table 1. Also, Crab nebula data were analyzed with the same code, with the derived flux and morphology consistent with previous measurements and the point-spread function, respectively. The distributions of the Hillas parameters for the excess events were checked and found to be consistent with Monte Carlo simulations for gamma-rays. The OFF-source data were compared with the Monte Carlo simulations for protons, and found to be consistent.

5. Discussion

The gamma-rays around 1 TeV are most likely produced by one of two mechanisms. We consider first the synchrotron/inverse Compton (IC) model. The spectra obtained using this model are shown in Fig. 3 (upper). This model has the following parameters: the magnetic field (B), the spectral index of electrons (γ), and the maximum electron energy ($E_{e,\max}$). The cutoff energy of the synchrotron emission is proportional to $E_{e,\max}^2 B$, which was constrained by the X-ray and the radio data. The cutoff of the IC emission is proportional to $E_{e,\max}^2$. The ratio of the peak of the synchrotron component and the peak of the IC component in the SED is proportional to B^2 . If B is too small, $E_{e,\max}^2$ is too high to explain our data, as shown by (a) in Fig 3. The lower limit of B in this model is $\sim 12 \mu\text{G}$ as shown by (b) in Fig. 3. This model cannot explain our data.

A more complex model in which the synchrotron and IC emissions come from different zones (a two-zone model) was considered by Aharonian, Atoyan, & Kifune (1997). At first, we assume the same electron spectra and B with different zone sizes. The lines(c) and (d) in Fig. 3 show the IC emissions with size ratios ($V_{\text{TeV}}/V_{\text{X-ray}}$) of 1 and $\sim 10^5$, respectively. The flux ratio between lines (c) and (d) corresponds roughly to the size ratio. This model requires a high size ratio and a strong magnetic field (~ 1.6 mG). *Chandra* observations revealed small-scale structures in the rim of SN1006 (Bamba et al. 2003): similar high resolution observations (in both X-rays and TeV gamma-rays) of RX J0852.0–4622 will help constrain the size ratio and refine this two-zone model. Stereo observations in the TeV region are required.

The other possible origin for the gamma-rays is π^0 decay. The estimated flux from π^0 decays is shown by the red line in Fig. 3 (lower). The emissions from the electrons were also considered using the electron/proton ratio (K_{ep}). Bremsstrahlung emission, shown by the green line, is constrained by the *ASCA* data. Therefore K_{ep} was limited to be at most 4×10^{-4} . As a result, both the flux of the inverse Compton emission and that of the bremsstrahlung were too small at TeV energies to explain our data. The sum of the π^0

emission, the inverse Compton emission and the bremsstrahlung is shown by the light blue line. The spectrum of accelerated protons is assumed to be a power-law with an exponential cutoff. The π^0 model has the following parameters: the spectral index of the protons, the maximum energy of protons ($E_{p,\max}$), and $A \equiv (E_0/10^{50}\text{erg})(n_0/\text{protons cm}^{-3})(d/0.5\text{kpc})^{-2}$, respectively. Here, E_0 , n_0 , and d are the total energy of protons in the region from which gamma-rays were detected, the number density of protons where the interactions occur, and the distance from the earth, respectively. The spectral index and the maximum energy of protons were assumed to be those of electrons, i.e., -2.5 and 8TeV , respectively. For the best-fit spectrum $A = 4.9$ was obtained. Assuming the distribution of the energy of the accelerated cosmic rays is isotropic, the total energy of accelerated cosmic rays in the whole SNR is proportional to the ratio $V_{\text{tot}}/V_{\text{TeV}}$, where V_{tot} is the total volume. This ratio was estimated to be 46 from the “significance map” with the assumption of spherical symmetry. The range of $E_0(V_{\text{tot}}/V_{\text{TeV}})$ of 10^{48} – 10^{50} ergs corresponds to n_0 of 23000–230, which are typical values for molecular clouds. Thus, the model of π^0 decays can naturally explain the multi-band spectrum.

The molecular distribution toward the whole extent of the Vela SNR has been mapped by Moriguchi et al. (2001). As RX J0852.0–4622 is embedded (in projection) in the Vela SNR, it is not possible to uniquely associate the detected molecular clouds with one or other SNR. The general anti-correlation of the X-rays and ^{12}CO with the Vela SNR suggests a strong interaction between this SNR and the interstellar medium, but does not rule out the existence of molecular clouds around RX J0852.0–4622, encouraging the further analysis.

This work was supported by a Grant-in-Aid for Scientific Research by the Japan Ministry of Education, Culture, Sports, Science and Technology (MEXT) of Japan, the 21st Century COE “Center for Diversity and Universality in Physics” from MEXT, the Australian Research Council, ARC Linkage Infrastructure Grant LE0238884, Discovery Project Grant DP0345983, and JSPS Research Fellowships. We thank the Defense Support Center Woomera and BAE Systems. We are indebted to Dr. H. Matsumoto for obtaining the X-ray spectrum.

REFERENCES

- Aharonian, F.A., Atoyan, A.M., & Kifune, T. 1997, MNRAS, 291, 162
 Aharonian, F.A., et al. 2001, A&A, 370, 112
 Aharonian, F.A., et al. 2004a, A&A, 425, L13

- Aharonian, F.A., et al. 2004b, *Nature*, 432, 75
- Aharonian, F.A. & Neronov, A. 2004, submitted to *ApJ*, astro-ph/0408303
- Aschenbach, B. 1998, *Nature*, 396, 141
- Aschenbach, B., Iyudin, A.F., & Schonfelder, V. 1999, *A&A*, 350, 997
- Bamba, A., Yamazaki, R., Ueno, M., & Koyama, K. 2003, *ApJ*, 589, 827
- Combi, J.A., Romero, G.E., Benaglia, P. 1999, *ApJ*, 519, L177
- Duncan, A.R. & Green, D.A. 2000, *A&A*, 364, 732
- Enomoto, R., et al. 2002a, *Astropart. Phys.*, 16, 235
- Enomoto, R., et al. 2002b, *Nature*, 416, 823
- Hillas, A.M. 1985, *Proc. 19th ICRC (La Jolla)*, 3, 445
- Hofmann, W. 2004, in *3rd Conf. on Frontier Science Proc.*, in press
- Itoh, C., et al. 2003, *A&A*, 402, 443
- Iyudin, A.F., et al. 1998, *Nature*, 396, 142
- Kawachi, A., et al. 2001, *Astropart. Phys.*, 14, 261
- Moriguchi, Y., Yamaguchi, N., Onishi, T., Mizuno, A., Fukui, Y. 2001, *PASJ*, 53, 1025
- Muraishi, H., et al. 2000, *A&A*, 354, L57
- Slane, P., Hughes, J.P., Edgar, R.J., Plucinsky, P.P., Miyata, E., Tsunemi, H., & Aschenbach, B. 2001, *ApJ*, 548, 814
- Tanimori, T., et al 1998, *ApJ*, 497, L25
- Tsuchiya, K., et al. 2004, *ApJ*, 606, L115
- Tsunemi, H., et al. 2000, *PASJ*, 52, 887

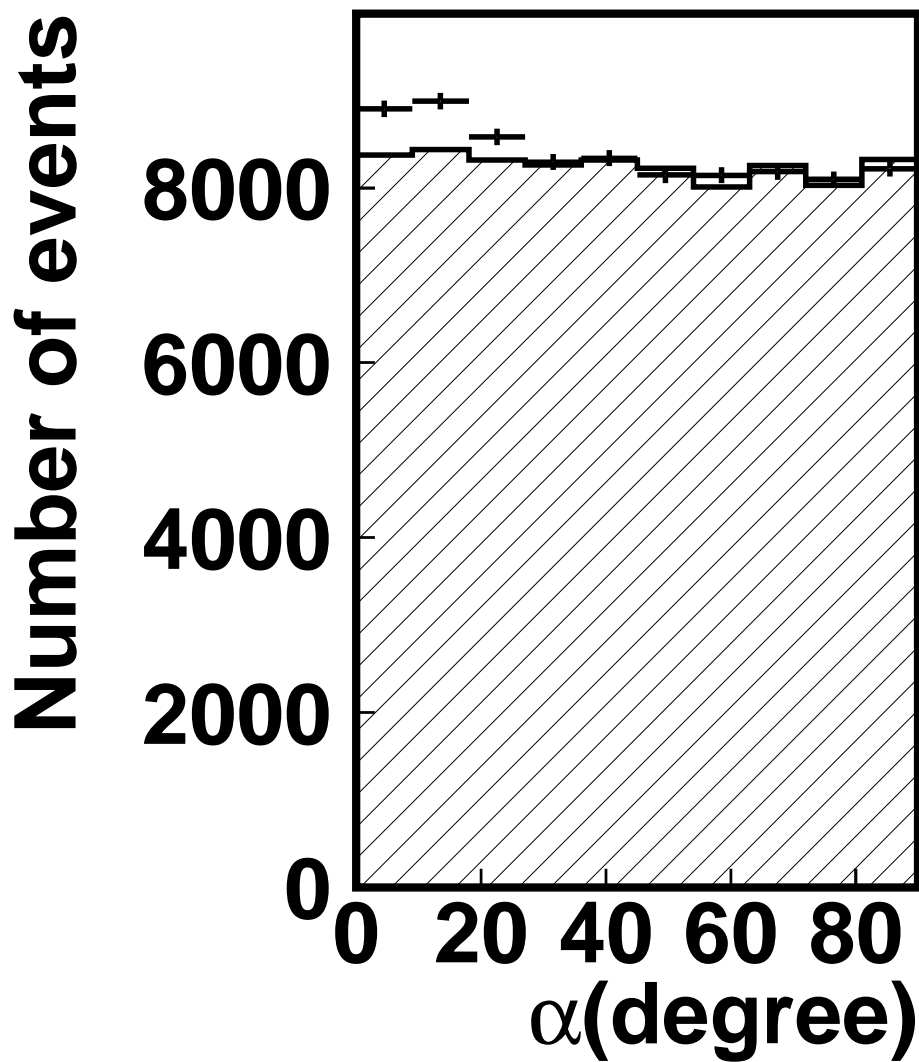


Fig. 1.— Distributions of α (image orientation angle) for the combined data in 2002 and 2003. The points with error bars show the ON-source data and the hatched histogram is the OFF-source data, which was normalized to the ON-source data using the number of the events with $\alpha > 27^\circ$.

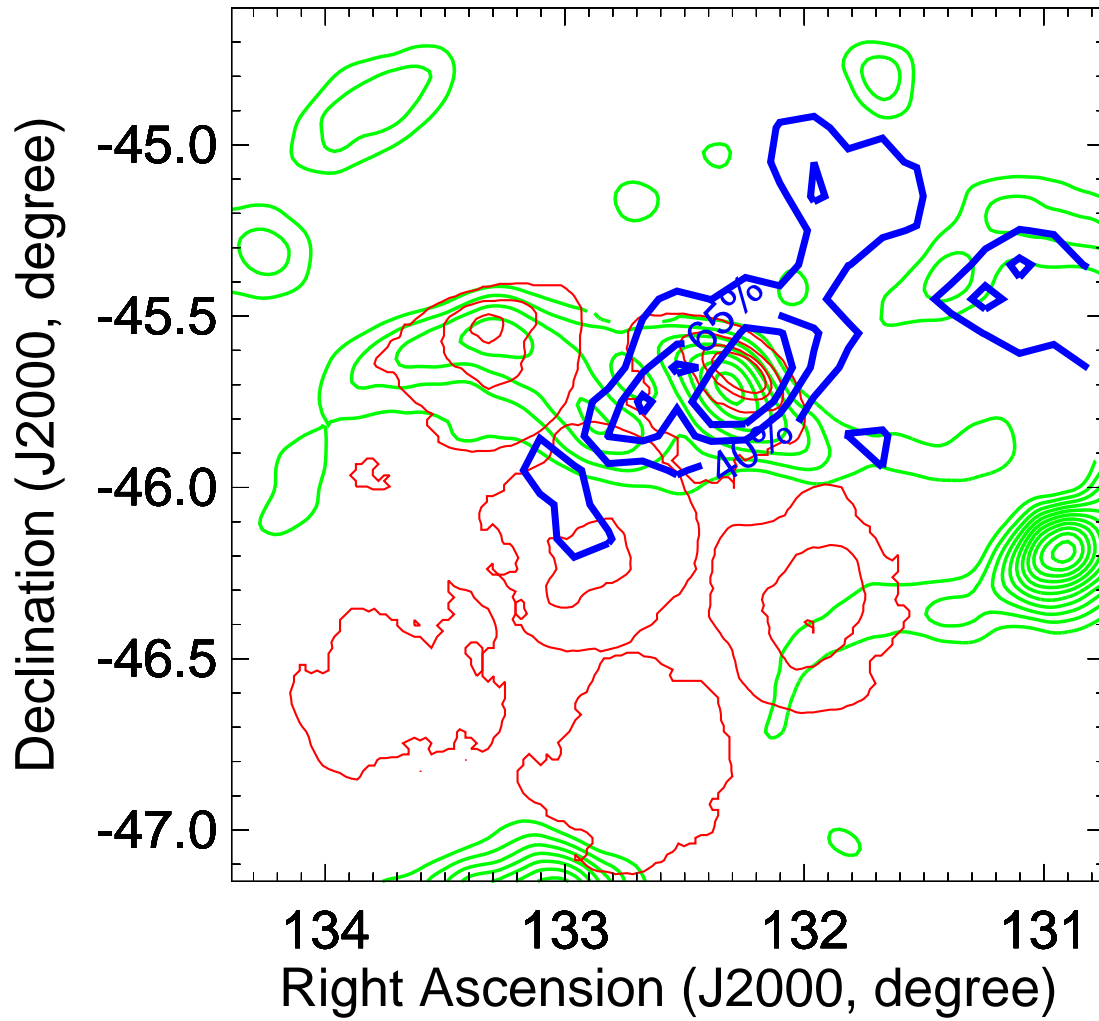


Fig. 2.— The “significance map” obtained by the CANGAROO-II telescope is shown by the blue contours. The telescope tracking center is at the north-west rim of RX J0852.0–4622. The red contours with levels at 20%, 45%, 65%, and 80% are an *ASCA* GIS image. The green contours show the 4850 MHz radio emission.

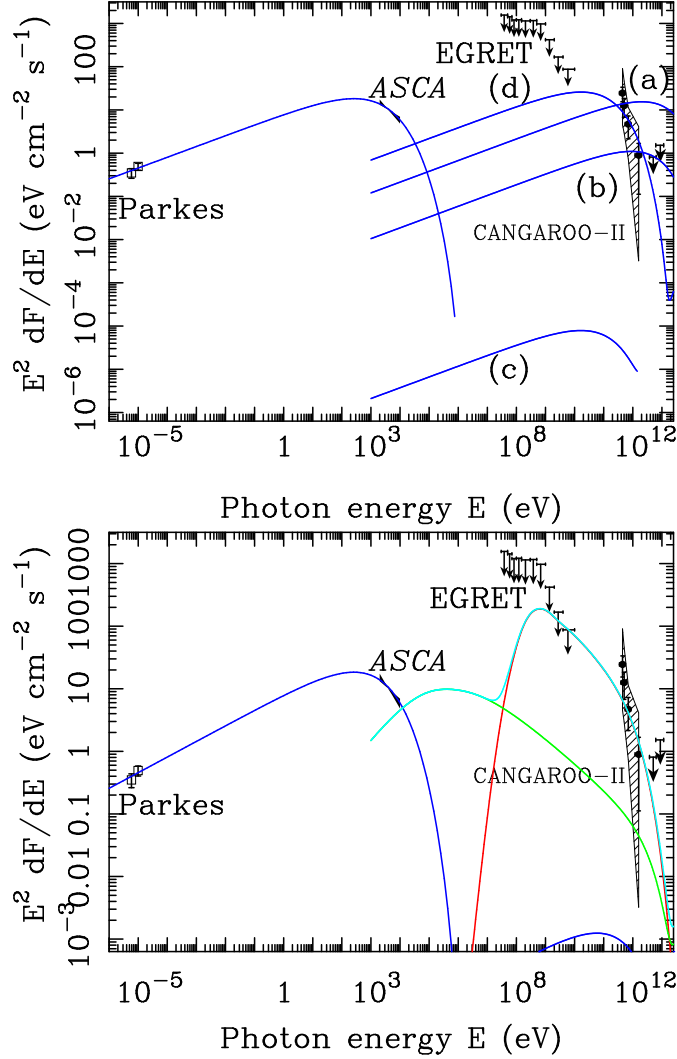


Fig. 3.— Spectral energy distribution of the north-west rim of RX J0852.0–4622. The points with error bars and the arrows in the TeV region are the fluxes and the 2σ upper limits, respectively, from our observations. The hatched area indicates the allowed region, where the χ^2 for the power-law fitting $< \chi^2_{\min} + 1$ including energy uncertainty, and χ^2_{\min} is the χ^2 for the best fit. The arrows around 100 MeV show the 2σ upper limits obtained using the EGRET data of the diffuse emission. They were derived from the count rate plus twice the standard deviation based on the archival data of the EGRET gamma-ray intensity map, which was integrated over the area considering the angular resolutions of EGRET and CANGAROO. The open squares with the error bars show the Parkes radio data (Duncan & Green 2000). The black filled areas show the *ASCA* X-ray data (Slane et al. 2001). The red line shows the estimation for π^0 gamma-rays, the details of which are given in the text. The blue lines shows the spectra of the various synchrotron/inverse Compton (IC) models. The green line shows the bremsstrahlung emission from electrons. The light blue line shows the sum of the π^0 , the inverse Compton, and the bremsstrahlung emissions.

Table 1: Differential fluxes.

Mean energy of bin [TeV]	Flux [ph/cm ² /s/TeV]	Lower bound*	Upper bound*
0.48±0.11	(9.43±3.49)×10 ⁻¹¹	1.99×10 ⁻¹¹	3.01×10 ⁻¹⁰
0.55±0.12	(3.85±1.78)×10 ⁻¹¹	1.03×10 ⁻¹¹	1.28×10 ⁻¹⁰
0.79±0.18	(8.54±4.63)×10 ⁻¹²	1.47×10 ⁻¹²	1.84×10 ⁻¹¹
1.93±0.48	(2.80±2.45)×10 ⁻¹³	1.35×10 ⁻¹⁵	1.22×10 ⁻¹²
5.84±1.51	3.18×10 ⁻¹⁴ **	—	—
10.38±3.15	1.91×10 ⁻¹⁴ **	—	—

*These were estimated where the χ^2 for the power-law fitting $< \chi_{\min}^2 + 1$ including energy uncertainty, where χ_{\min}^2 was the χ^2 for the best fit.

**These are 2σ upper limits.